Mechanical Analysis and Design of Large Building Integrated Photovoltaic Panels for a Seamless Roof

Linda G. Teka[a], Mehdi Zadshir[a], Huiming Yin [1a]

[a]*Department of Civil Engineering and Engineering Mechanics, Columbia University, 610 Seeley W. Mudd 500 West 120th Street, New York, 10027, NY, USA*

Abstract

When a large building integrated photovoltaic (BIPV) panel is subjected to surface loading, due to the small thickness and large span of the building pane, the high transverse deflection often becomes the control factor in the structural design. To reduce the deflection, thick glass sheets are required to provide sufficient flexural rigidity, which increases the dead load thereby leading to inefficient design. This paper investigates a new stiffening mechanism for BIPV panels by imposing horizontal constraints along the supporting edges, which is required to minimize the gap between panels for leakage control and lifetime extension of the building envelope. Given a transverse load on the panel surface, the horizontal constraint will reduce the deflection at the center of panels, a new governing equation is formulated and the solution is derived for different boundary conditions. For a large BIPV panel with simple supports on two opposite edges with a linear horizontal constraint, the deflection of the panel can be predicted by the nonlinear elastic theory, which aligns well with the previous experiments. The model is extended to other boundary conditions and shows that the horizontal constraint on clamped panels can further reduce the deflection, which results in making the BIPV panels thinner. The present formulation is useful in the design and analysis of BIPV systems. A new BIPV mounting system based on the present theory is proposed to provide tailorable stiffness and adaptive control of the panel gap for the longevity of the BIPV systems.

Keywords: Building integrated photovoltaic (BIPV), solar panel, smart mounting system, membrane force, beam theory, nonlinear elastic deformation

Nomenclature

μ Spring stiffness

[1]Corresponding author. Tel.: +1 (212) 851-1648, Email address: yin@civil.columbia.edu

$\overline{EA}$ Effective axial rigidity

$\overline{EI}$ Effective flexural rigidity

$BAPV$ Building applied photovoltaic

$BIPV$ Building integrated photovoltaic

$CCFF$ Clamped on two opposite edges and free on the other two edges

E Young's modulus

EVA Ethyl vinyl acetate

I Moment of inertia

P Axial load

PV Photovoltaic

q Transversely distributed load

$SSFF$ Simply supported on two opposite edges and free on the other two edges

w Transversal deflection

1. Introduction

A building integrated photovoltaic (BIPV) system generally consists of solar cells or modules that are integrated into building elements as part of the building structure[1]. It is typically manufactured by packaging solar cells between a transparent glass surface layer and the structural substrate layer by an encapsulant. The substrate can be fiber reinforced concrete panel or glass sheet as well. It is different from the traditional building applied photovoltaic (BAPV) system as it is an integrated part of the building structure with load resistance instead of an attachment to the roof[2]. When the paradigm of energy generation keeps changing, it is important to investigate the variety of materials and products available in building design.

BIPV modules not only generate electricity but are an integrated part of the building structure that transfer loads to the building framework and the foundation while providing sun protection, thermal insulation, noise protection, and safety to the building. Building integrated photovoltaic (BIPV) panels are subjected to environmental and dead loads, such as wind, snow, impact loads,

and thermal loads due to daily or seasonal temperature changes[3–5]. These loads will cause stress and deformation, which may lead to undesirable aesthetic appearance, visual perception of damage (sagging), cell cracking, panel delamination, permanent deformation, or panel failure [1, 6]. Therefore, the correct prediction of deflection and stress of BIPV panels is essential during the building structural design, particularly when large modules with the size of $1m \times 2m$ or greater [1] are often used in modern structures today. Since the glass sheet is very thin, the panel undergoes considerable deflections due to the low bending rigidity [1, 7–9].

The mechanical behaviors of BIPV panels, including loading capacity, deflection, stress distribution, etc., directly impact the functionality, aesthetics, and safety of the building [1, 10]. However, the mechanical behavior of BIPV panels has not been extensively studied, and only a few scholars have carried out related research on the mechanical properties of BIPV, which mainly focused on the mechanical properties of solar cells themselves, and not as a multilayered glass laminated structure [10, 11]. To date, no specific building code exists to address the unique geometry and mechanical behavior for the PV modules applied to the BIPV systems [8, 11]. Although IEC 61215 [12] has addressed the mechanical behavior of a single module for strength and toughness under an accelerated testing environment, it does not address the structural loads yet. The recent published IEC 63092 [13, 14] specifies that BIPV systems shall withstand the loads that can be verified either by calculation or by testing, but the nonlinear elastic behavior of BIPV panel is not addressed. Currently, existing building codes for general building materials are used in the BIPV designs but often lead to an overly conservative design with thick panels [15].

BIPV modules generally consist of multi-layers of glass, photovoltaic (PV) cells, backsheet or substrate packaged with a softcore of an encapsulant, such as ethylene-vinyl acetate (EVA), polyvinyl butyral (PVB), polydimethylsiloxane (PDMS) elastomer, thermoplastic polyolefin (TPO) elastomer, and Ionomers. The softcore protects PV cells from in-plane deformation by tension or compression, but the bending of a module may lead to microcracks of cells and the loss of energy harvesting efficiency. Some of the research that has been done to study the mechanical properties of BIPV panels include investigating the mechanical behavior of a PV module, assembled by a glass-EVA-glass laminate. Dietrich et al carried out experiments and finite element analysis to observe the effect of the EVA layer and the placement of the clamps [16]. The test results showed that the stiffness of large photovoltaic panels is affected by the stiffness of EVA. The work done by Sable et al[17] investigated the mechanical behavior of different laminates, mainly ethylene vinyl acetate (EVA), and polyvinyl butyral (PVB), for layered glass structures. By conducting four-point loading

tests and finite element modeling [17], the results showed that the stiffness of the glass laminates with EVA is similar to the stiffness of the PVB laminated glass structures.

Due to the differences in material properties of the constituting materials and the relatively low thickness of the soft core, it is challenging to predict the complicated mechanical behavior of these panels[18]. BIPV panels exhibit high contrast of material properties; the stiffness ratio of glass to encapsulant is approximately 1000:1 and the thickness ratio of glass to PV cell is at least 100:1, and the width-thickness ratio is no less than 100:1, making it difficult to model the stress transfer through the panel[1, 8]. Consequently, layer-wise composite models [18–21] were proposed to study the stress and deflection of laminated glass panels by treating BIPV panels as a layered composite with two stiff skin layers and a soft core [8]. Additionally, the theory was extended to unsymmetrical laminated beams [22] by using the layer-wise theory to build the constitutive equations, and the formulation was verified by the three-point bending test. For curved laminated glass and photovoltaic structures, the layer-wise theory was also used for the analysis by using the analogy to the existing theories of plates [5].

The layer-wise models for laminated glass beams with PVB are presented in [9] with the assumption that glass skin layers deform according to the Bernoulli–Euler beam theory. The model is derived by variational principle from the membrane and bending strain energy of the glass layers and the shear strain energy of the PVB-interlayer.Based on the boundary conditions, the behavior of laminated glass beams under large deflections could be either linear for simply supported beams or nonlinear for beams with fixed support. The Kirchhoff–Love and Reissner–Mindlin plate theories [23] are the two most common dimensionally reduced models of a thin linearly elastic plate. The Reissner–Mindlin model is more accurate, particularly for moderately thin or thick plates and when transverse shear plays a significant role, but the improvement is not substantial for very thin plates [24], which is the case for BIPV applications.

The existing theories and models commonly predict that the deflection of the panels linearly increases with the loading when the stress in the panel is in the linear elastic range. However, strong nonlinear deflection of the solar panels has been observed in the experiments [3, 8], which means that the linear models will overly design the thickness of the panel. Accordingly, a larger glass thickness means a higher dead load and material cost, which is not efficient. Accurately predicting the nonlinear deformation will improve the design of solar panels for lightweight, economic BIPV systems. Particularly, using the horizontal constraints to reduce the deflection can be another stiffening mechanism for BIPV panels, so that thinner glass sheets can be used for the same maximum

deflection specification.

When a BIPV panel under transverse loading is supported by two beams along the two opposite edges, the module exhibits cylindrical bending and the deformation can be predicted by the beam theory [24, 25]. Because the panel's width and span are much larger than the thickness, the deflection of the panel can be large. The connections between the panel and beam are required to be seamless to avoid leakage problems [1]. Therefore, depending on the contact between the panel and the supporting beam, the boundary condition can be either simple or clamped supports with horizontal constraints. Rubber or silicone cushions are commonly used to reduce stress concentration and provide waterproof insulation, which provides horizontal force to hold the connection but exhibits certain flexibility for stress relaxation [26, 27]. However, the lifetime of the cushion depends on the loading cycles and magnitude, which eventually leads to fatigue and cracking of the material .

On the other hand, he mounting system of PV modules has an impact on the mechanical properties of the modules. Afinite element method (FEM) simulation done [28] on the thermo-mechanical assessment of different mounting systems, including the clamping of framed and unframed PV laminates, concluded that the frameless clamped PV laminate shows a significantly larger displacement of 147mm compared with the framed PV module with 54mm displacement for a 2.4KPa force. In addition, due to the mechanical stress induced on the panels, the unframed laminate has a wave-like deflection; whereas the framed laminate, due to the support along all edges exhibits an elliptic deflection.

Photovoltaic structures have also been analyzed by finite element modeling and simulation [8, 16, 17]. Due to differences in material properties, stiff and brittle glass and soft EVA layer, and the high thickness ratio of glass to EVA, it is challenging to reach a stable and convergent prediction of the actual structural behavior [20], particularly, when the load is large. The horizontal constraint from the support frame may significantly change the deflection and lead to nonlinear deformation. Moreover, a strong horizontal constraint can control the gap between two neighboring panels under the same transverse loading, and improve its performance for leakage resistance.

Indeed, the ultimate resistances and failure patterns of beams can be greatly altered by the effects of the membrane force introduced by special constraints. The experimental work done by Chen et al [29] on hybrid fiber reinforced-lightweight aggregate concrete (HFR-LWC) beams, investigated the effect of membrane forces on the capacities of the beams, by introducing membrane forces through specifically designed clamps. The experimental results showed that the ultimate

load of the beams could be substantially underestimated if membrane forces were neglected. A simplified membrane action theory was presented by modifying the maximum membrane force design method (MMFM) for predicting the total static resistance-deflection curves of restrained beam-slab reinforced concrete (RC) structures [30]. In addition, the experimental tests were conducted on constrained beams, and the results showed that the static load-carrying capacity and membrane force increased with increasing restraint stiffness. The analytical solution for estimating the capacity of fully clamped slabs was suggested [31] by incorporating the membrane action and its contribution to the load-carrying capacity of the clamped slab. The report indicated that the load-deflection relationships of fully clamped RC slabs can be reasonably depicted by taking compressive-tensile membrane effects into account. However, the nonlinear analysis [30] focused on the elastoviscoplastic material behavior, which is not dominant in glass modules.

This paper investigates the nonlinear deformation of large panels with horizontal constraints. When a large panel is simply supported at the two opposite edges with a rubber-cushioned clinch and is free on the other two edges (SSFF) [3], the clinch provides both horizontal and vertical constraints. The membrane force caused by the horizontal force will reduce the curvature and lead to nonlinear deformation of the panel. The proposed model will address this problem and build a foundation for future BIPV panel design. In the following, the problem of a large BIPV panel supported by two opposite edges is proposed, and the elastic analysis provides the governing equation and general solution. For the SSFF boundary condition, the solution can predict the existing experimental results very well. It is then extended to the boundary condition with two clamped, two free edges (CCFF). The parametric analysis is conducted for the optimal design of the BIPV panel and its mounting system. By controlling the horizontal constraint, one can design lightweight, stiff BIPV systems to meet the design requirements. A new mounting system is introduced with the present theory that will provide tailorable stiffness and adaptive control of the panel gap for the longevity of the BIPV systems [32].

2. Problem statement

Consider a simply supported solar panel with two free edges under a distributed static transverse load as shown in Figure 1(a) [8]. Due to the symmetry of the loading and geometric configuration, the panel exhibits cylindrical deformation approximately, which can be represented by the cross-section in Figure 1(b). When the load is zero, the panel stays straight. As the load increases, the cylindrical deformation in three dimensions (3D), which can be represented by a flexural de-

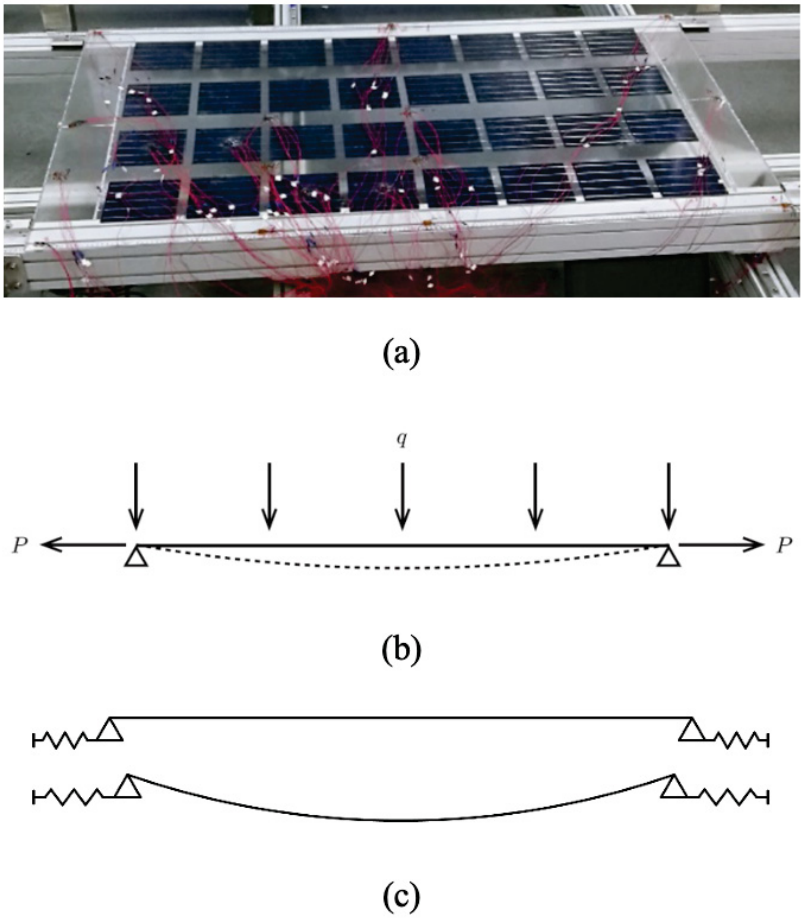

Figure 1: Schematic illustration of a simply supported solar panel: (a) solar panel supported by the frame along two opposite edges [8]; (b) the cylindrical deformation simplified by a beam with the 2D cross-section, and; (c) the slip of the panel at the simple supports simulated by a linear spring.

formation in 2D, results in beam bending. The length change of the curved beam will lead to a membrane force along the span of the panel, which will carry a certain load similar to a cable in suspension bridges. The change of the force coupled with the curvature of the beam leads to a nonlinear deformation. However, existing design practices often use classic beam or plate theory [1, 8], and the nonlinear elastic behavior is not taken into account. Note that although the solar panel in Fig. 1(a) is smaller than those large solar panels used in the modern structures today, it clearly exhibits nonlinear elastic behavior which will be demonstrated subsequently in Section 4 [8].

Moreover, to protect glass from fracture by stress concentration, the clinch of simple support cannot be perfectly rigid. In general, the rubber cushioned clinches allow slight slip for stress relaxation and leakage prevention. For simplicity, the in-plane force is assumed to linearly increase

with the slip in Figure 1(c), which can be simplified as a linear spring. In addition, although PV panels are typically layered materials with glass, encapsulant, and substrate layers, they can be approximated by a uniform beam with an effective flexural rigidity, which can be measured experimentally or estimated by stress analysis.

In summary, the following assumptions are proposed to simplify the physical problem of a BIPV panel under the SSFF configuration.

- The material behavior is linear elastic for the local stress-strain relationship.
- The plate is simplified by a 2D composite beam with an effective flexural rigidity $\overline{EI}$.
- The plane assumption in the classic plate or beam theory is used for linear strain distribution along the thickness.
- The elastic cushioned supports are modeled with a linear elastic spring of stiffness μ. When $\mu \to \infty$, it is perfectly rigid; when $\mu \to 0$, it becomes a roller.

In the above assumptions, all constitutive models are linear elastic, which can be characterized in the experiments. However, the kinematics will be nonlinear if the bending and stretching mechanisms interplay. The nonlinear effect will be rigorously analyzed and predicted in the following section.

3. Formulation

3.1. Governing equation and general solution

Under a uniformly distributed load q, a beam of length L undergoes a deflection $w(x)$ in the downward direction thus producing a horizontal force P in the axial direction. Figure (2) shows the equilibrium of an infinitesimal element of the beam. The shear force V and moment M vary with x while the horizontal force P is independent of x as there is no external horizontal force. Therefore, the force equilibrium along x is satisfied. The equilibrium of forces along the y direction and the bending moment can be written as:

$$\frac{dV}{dx} = -q \tag{1}$$

$$V = \frac{dM}{dx} + P\frac{dw}{dx} \tag{2}$$

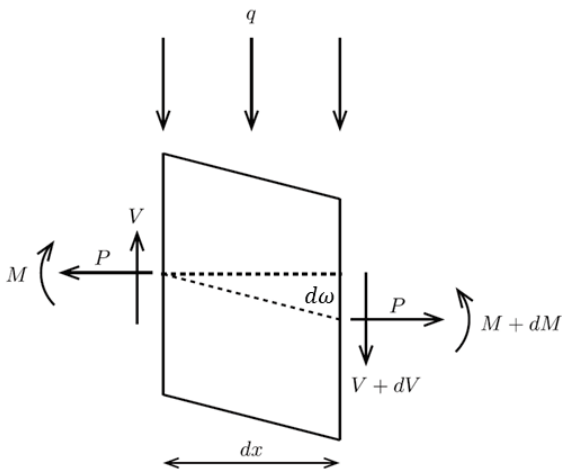

Figure 2: Free body diagram of an infinitesimal beam element

According to the moment-curvature relation,

$$M = -\overline{EI}w'' \tag{3}$$

where $\overline{EI}$ is the effective flexural rigidity which will be elaborated in the next section.

By combining Eqs. (1-3), the governing equation can be written as [23],

$$\overline{EI}\frac{d^4w}{dx^4} - P\frac{d^2w}{dx^2} = q \tag{4}$$

To simplify the derivation, a dimensionless parameter is defined as $u^2 = \frac{PL^2}{4\overline{EI}}$. The above equation can be rewritten as

$$\frac{d^4w}{dx^4} - \left(\frac{2u}{L}\right)^2 \frac{d^2w}{dx^2} = \frac{q}{\overline{EI}} \tag{5}$$

Therefore, the general solution is obtained as

$$w(x) = C_1 \sinh\frac{2ux}{L} + C_2 \cosh\frac{2ux}{L} + C_3x + C_4 - \frac{qx^2}{2P} \tag{6}$$

where C_1, C_2, C_3 and C_4 are constants that can be determined by using the boundary conditions.

In comparison with the classic Bernoulli–Euler beam theory, the second term related to p or u, in Eq. (4) or (5), respectively, is not considered, and a polynomial general solution is obtained instead with the cubic and quadratic terms corresponding to C_1 and C_2, respectively.

3.2. Deflection function for the SSFF boundary condition

For a simply supported beam, the boundary conditions are given by the deflection and moment at the supporting ends as

$$w(0) = w(L) = 0 \tag{7}$$

$$w''(0) = w''(L) = 0 \tag{8}$$

The four boundary conditions can be used to determine C_1, C_2, C_3 and C_4 as follows

$$C_1 = \frac{qL^4}{16u^4\overline{EI}}\left(\frac{1-\cosh 2u}{\sinh 2u}\right); C_2 = \frac{qL^4}{16u^4\overline{EI}}; C_3 = \frac{qL^3}{8u^2\overline{EI}}; C_4 = -\frac{qL^4}{16u^4\overline{EI}} \tag{9}$$

Therefore, the solution in Eq(6) is determined as

$$w(x) = \frac{qL^4}{16u^4\overline{EI}}\left(\frac{1-\cosh 2u}{\sinh 2u}\sinh\frac{2ux}{L} + \cosh\frac{2ux}{L} - 1\right) - \frac{qL^2x^2}{8u^2\overline{EI}} + \frac{qL^3x}{8u^2\overline{EI}} \tag{10}$$

With the aid of hyper trigonometric relation, Eq(10) is rewritten as

$$w(x) = \frac{qL^4}{16u^4\overline{EI}}\left(\frac{\cosh u\left(1-\frac{2x}{L}\right)}{\cosh u} - 1\right) + \frac{qL^2x(L-x)}{8u^2\overline{EI}} \tag{11}$$

After deformation, the beam exhibits curling and slope θ, and the horizontal length projection is;

$$L_x = \int_0^L \cos\theta ds \tag{12}$$

Where ds is the infinitesimal curve length along the deformed beam, and $cos = dx/ds$. The horizontal length change, λ under the small deformation assumption is then calculated as,

$$\lambda = L - L_x = \int_0^L (1-\cos\theta)ds \approx \int_0^L \frac{1}{2}\left(\frac{dw}{dx}\right)^2 dx \tag{13}$$

which means that if the beam's length does not change but its shape changes with deflection $w(x)$, the horizontal length must shrink by λ. However, the horizontal constraint will reduce the motion of the ends. Based on the displacement compatibility, the length change λ includes two parts: the elongation of the beam and the displacement of elastic support as follows

$$\frac{PL}{\overline{EA}} + \frac{2P}{\mu} = \lambda \tag{14}$$

where $\overline{EA}$ is the effective axial rigidity. Combining Eqs. (11), (13), and (14) produces the characteristic equation of u, written as

$$\frac{4(\overline{EI})^3u^2}{\overline{EA}L^8q^2}+\frac{8(\overline{EI})^3u^2}{\mu L^9q^2}=\frac{5}{256}\frac{\tanh u}{u^7}+\frac{1}{256}\frac{\tanh^2 u}{u^6}-\frac{5}{256u^6}+\frac{1}{384u^4} \tag{15}$$

Eq.(15) exhibits multiple solutions of u, but only one has a physical meaning, from which P can be obtained by Eq. (11). To solve the physical root of u, when $\mu \to 0$ it is reduced to a roller support with $P = 0$ or $u = 0$, and the length change of the beam can be zero. When $\mu \to \infty$, it is an ideally simple support with a zero-horizontal displacement. The classic Euler Bernoulli (B-E) beam provides the deflection function as

$$w=\frac{qx}{24\overline{EI}}(x^3-2Lx^2+L^3) \tag{16}$$

Using Eq. (16) in Eq. (13), one can obtain $\lambda = \frac{17q^2L^7}{70(24)^2\overline{EI}^2}$, which provides $P = \frac{17q^2L^6\overline{EA}}{70(24)^2\overline{EI}^2}$ from Eq. (14). Because the B-E beam does not consider the effect of λ, Eq. (16) cannot catch the nonlinear elastic behavior of the beam as w linearly varies with q. However, because it overly estimates w(x), the actual length change shall be smaller, and $P < \frac{17q^2L^6\overline{EA}}{70(24)^2\overline{EI}^2}$. Therefore, Eq.(5) provides $0 < u < \sqrt{\frac{17\overline{EA}}{70\overline{EI}}\frac{qL^4}{48\overline{EI}}}$, which defines the range of u. Once the value of u is numerically solved in Eq. (15), the analytical solution is fully obtained in Eq. (16).

3.3. Deflection function for the other boundary conditions

Following the same procedure, the formulation can be extended to beams with various boundary conditions. For example, a BIPV panel with two clamped, two free edges (CCFF) can be idealized as a clamped beam, where both ends of the beam are restrained against the vertical and rotational motion will be discussed further in the following section. For a clamped beam, the boundary conditions are:

$$w(0)=w(L)=0 \tag{17}$$

$$w'(0)=w'(L)=0 \tag{18}$$

The general solution of Eq. (6) can be applied to the four boundary conditions to determine C_1, C_2, C_3 and C_4 in a similar fashion as the last subsection:

$$C_1=\frac{-qL^4}{16u^3\overline{EI}};C_2=\frac{qL^4}{16u^3\overline{EI}}\left(\frac{1+\cosh 2u}{\sinh 2u}\right);C_3=\frac{qL^3}{8u^2\overline{EI}};C_4=-\frac{qL^4}{16u^3\overline{EI}}\left(\frac{1+\cosh 2u}{\sinh 2u}\right) \tag{19}$$

Therefore, the deflection is determined as

$$w(x) = \frac{qL^4}{16u^3\overline{EI}} \frac{\cosh u \left(1 - \frac{2x}{L}\right) - \cosh u}{\sinh u} + \frac{qL^2 x(L-x)}{8u^2\overline{EI}} \tag{20}$$

Similarly, as in the case with the simply supported beam, we will find the characteristic equation of u by using Eqs. (6), (13), (14), and (19).

$$\frac{4\overline{EI}u^2}{\overline{EA}L} + \frac{8\overline{EI}u^2}{\mu L^2} = \int_0^L \frac{1}{2}\left(\frac{dw}{dx}\right)^2 dx \tag{21}$$

Analogously, to find a meaningful u, when $\mu \to 0$; $P = 0$ or $u = 0$, and the deflection is obtained as the classic beam as $w = \frac{qx^2}{24\overline{EI}}(L-x)^2$ and then $\lambda = \frac{q^2L^7}{105(24)^2\overline{EI}^2}$. Therefore, one can obtain $P < \frac{q^2L^6\overline{EA}}{105(24)^2\overline{EI}^2}$ or $0 < u < \sqrt{\frac{\overline{EA}}{105\overline{EI}}}\frac{qL^4}{48\overline{EI}}$. Compared with the SSFF, the quantity of P or u is much smaller for the CCFF due to the constraint of the rotational angle.

Finally, the value of u can be numerically solved using Eq. (21), and subsequently, the deflection can be calculated using Eqs. (6) and (19).

For other boundary conditions, such as one edge simply supported, and one edge clamped (SCFF or CSFF), the same procedure can be applied. Once the deflection curve is solved, the stress distribution over the beam can be written as:

$$\sigma_{xx} = E(y)\left(-y\frac{d^2w}{dx^2} + \frac{P}{\overline{EA}}\right) \tag{22}$$

where the horizontal force from the support provides a uniform stress while the moment on the beam provides a linearly distributed stress along the cross-section.

Note that $\overline{EA}$ and $\overline{EI}$ are the effective axial stiffness and flexural rigidity of the cross section of the beam, respectively, which can be experimentally measured. Traditional composite beam theory assumes that the cross section stays in the same plane during the deformation. Eq. (22) follows the traditional composite beam assumption. However, because the soft core of the EVA layer may not bend together with the two stiff layers [5], the composite beam theory will overestimate the flexural rigidity, which can be measured by experiments instead.

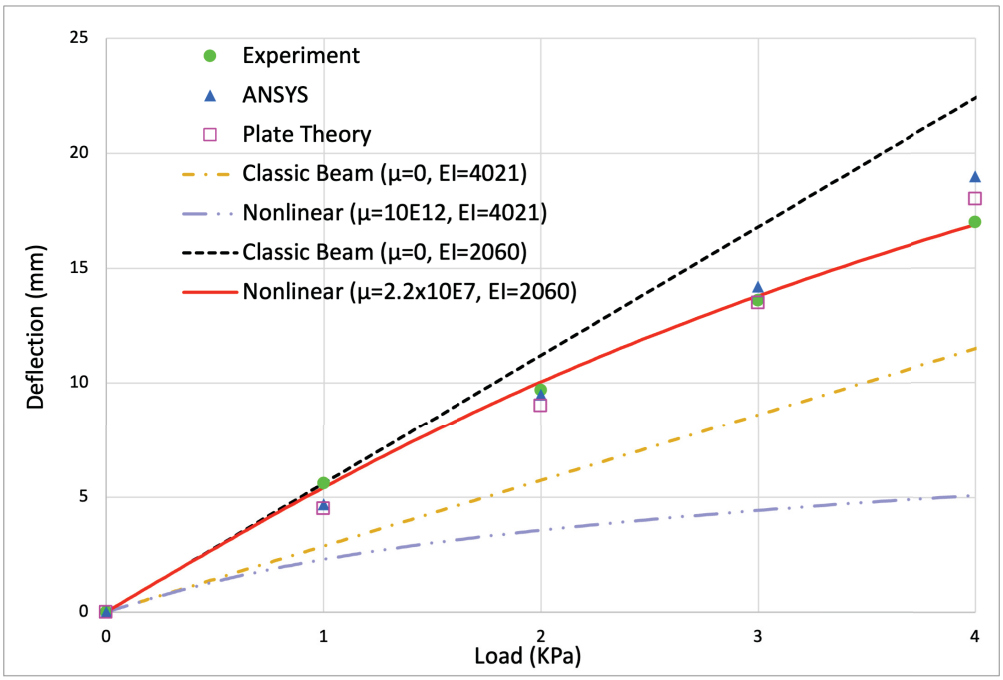

Figure 3: The deflection of the center versus the load for an SSFF BIPV panel for the model validation with the experiments [8].(EI is in $N.m^2$)

4. Results and Discussion

4.1. Validation with the experimental results for SSFF panels

The above formulations can be used for general SSFF and CCFF configurations of BIPV panels with cylindrical deformation, such as glass panels and laminates. To validate the formulation, we apply the formulation in comparison with the experimental data for the SSFF configuration in Li et al [8]. The dual glass solar module in Figure 1(a) exhibits a size of $1658 \times 855 \times 7.4$ (mm^3) as a glass-EVA-glass laminate. The thin silicon cells are embedded in EVA with a certain spacing between them, and EVA serves a protective layer to reduce the stress transfer from the structure to PV cells, which reduces microcracking and efficiency loss of the solar cells. Therefore, the PV cells can be ignored in the mechanical analysis although it is the key for energy harvesting. The material properties of the constituent layers are tabulated in Table 1.

Material	Glass	EVA
Young's Modulus (MPa)	7.2×10^4	35
Poisson Ratio	0.2	0.3
Thickness (mm)	3.2	1

Table 1: Material properties of the layers in the dual-glass BIPV module

However, neither the finite element simulation with ANSYS nor the previous plate theory in Li et al. [8] can capture the nonlinear trend of the experimental data for the deflection changing with the load in Figure 3. The ANSYS and plate theory underestimate the deflection for small loading but overestimate it for large loading. The plate theory exhibits a linear trend; the ANSYS can be slightly nonlinear; whereas the experimental results are significantly nonlinear.

Using the material constants in Table 1, for a classic composite beam, we can calculate the flexural rigidity $\overline{EI} = 4021\text{N.m}^2$ and axial rigidity $\overline{EA} = 764.1 \times 10^6\text{N}$. Using them in Eqs. (15) and (16), we can calculate the deflection. When $\mu \to 0$, no horizontal constraint can be provided by the support, the present theory provides the same prediction as the classic beam, which is linear. When $\mu \to \infty$ (numerically $\mu = 10^{12}\text{N/m}$ used), the horizontal deformation is fully constrained and nonlinear behavior is observed. However, the deflection calculated in both cases is much smaller than the experimental values. This is due to the soft core of EVA encapsulated in between the glasses. The EVA interlayer cannot transfer sufficient shear stress to maintain the cross-section in-plane, therefore the effective flexural rigidity of the composite beam will be much smaller than the classic composite beam as the plane assumption in the cross-section is not valid anymore. The experimental work [16] also shows that the stiffness properties of the EVA layer directly influence the stiffness of the PV module.

Because the effect of the soft core on the effective flexural rigidity $\overline{EI}$ of the BIPV panel is fairly complex, the plane assumption in the classic beam is not accurate anymore [5, 18], which may overestimate the flexural rigidity. Alternatively, it is more straightforward and reliable to determine the value of $\overline{EI}$ experimentally. Otherwise, we can use the experimental data to calibrate the $\overline{EI}$ value: When the load is small, the nonlinear effect is negligible, so the linear relationship between the deflection and the load can be used to back-calculate the effective flexural rigidity. Hence the true effective flexural rigidity can be calibrated by using the experimental data in the linear range in [8], i.e. the point where 1KPa loading, and 5.6mm deflection, at which the point the $\overline{EI}$ value is calibrated to be $\overline{EI} = 2060\text{N.m}^2$. Considering the elastic support to be $\mu \approx 22 \times 10^6\text{N/m}$, we can estimate the deflection at the center of the panel with the solid line, which agrees with the experimental data very well. Compared with the classic beam theory or the case at $\mu = 0$, the nonlinear result for the load at 4KPa is more than 20% lower. Because the physical meanings of $\overline{EI}$ and μ are clear, they can be measured by other methods as well.

The results from the classic beam and the nonlinear models are close to each other for small loads, but as the load increases, the deflection that is calculated from the nonlinear model is much

less than the results from the classic beam theory. This stiffness is the result of the large membrane force created due to the horizontal constraints. The stiffness of the elastic support μ may change the nonlinear behavior significantly. The classic beam or plate theory or finite element method does not consider the effect and thus cannot capture the nonlinear behavior well.

4.2. Effect of the types of the boundary condition

The last subsection shows that the simple supports with horizontal constraint stiffen the BIPV panel for deflection in comparison with the case with roller supports. The stiffening effect depends on the spring coefficient μ of the constraint, which will be elaborated on in the next subsection. The boundary condition type also plays a significant role in deflection. A clamped beam with horizontal constraint will be investigated. When $\mu \to 0$, no horizontal constraint can be provided by the support, and the beam is only constrained by the rotational angle and deflection; when $\mu \to \infty$, the beam's ends are fixed by the rotational angle, deflection, and horizontal displacement. The classic beam theory typically ignores the effect of the horizontal constraint, therefore, the effect of μ is not taken into account. For the framed BIPV panel, the rotational angle at the support edge is indeed constrained by fixing the frame onto the supporting beam, and the rubber cushion between the glass layer and the frame can provide a certain horizontal force against the horizontal motion. The present formulation for a CCFF beam can address the problem and evaluate the effect of the horizontal constraint.

Figure 4 shows the deflection of a clamped beam (CCFF) and a simply supported beam (SSFF) by comparing the classic beam deflection to nonlinear deflection. As expected, the deflection of the CCFF beam calculated from the formulation is nonlinear, similar to but less than that of the SSFF beam. The non-linearity is more apparent as the axial tensile load increases, proving that the formulation captures the true nonlinear deformation of BIPV panels and shows the significance of the effect of membrane force on the deflection of solar panels. Because the CCFF exhibits stronger support to the panel with additional rotational constrain, the deflection is significantly smaller than SSFF at the same transverse loading. Therefore, the nonlinear solution is fairly close to the classic linear one in the range shown in the figure. Given an allowable deflection, the CCFF will provide a much higher load capacity than SSFF. Compared with the experiments in the last subsection, when a load of 4KPa is applied, the horizontal constraint does not show an effect on the deflection for the CCFF panel but reduces 20% of the deflection at the center for the SSFF panel. When the loading range is larger, the nonlinearity of CCFF will become apparent, which will be shown

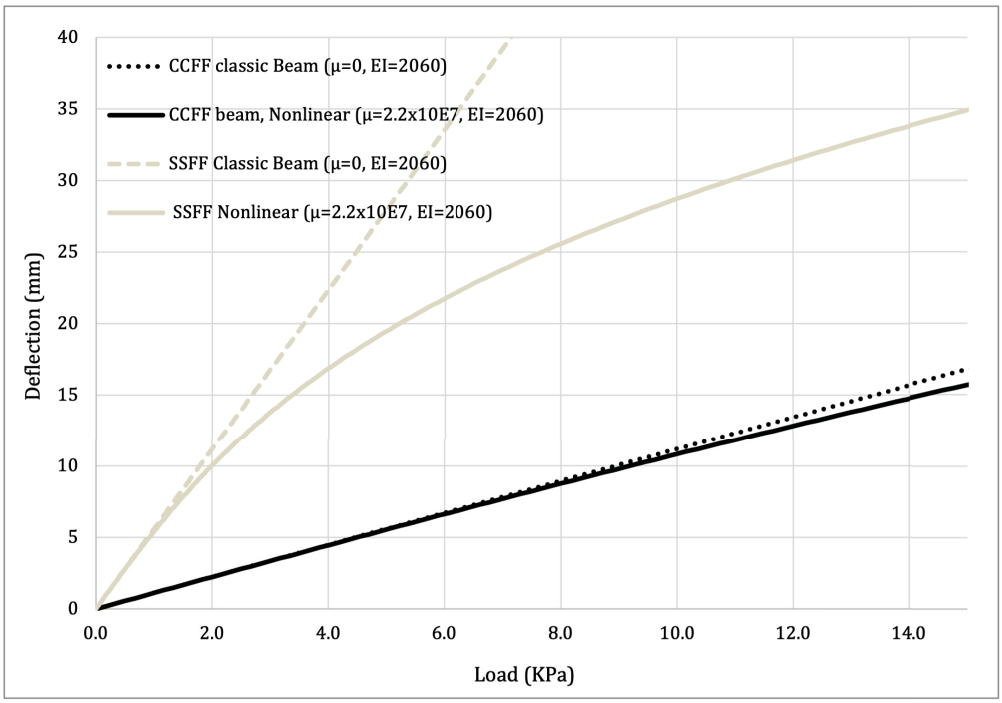

Figure 4: The deflection of the center versus the load for SSFF and CCFF BIPV panels

subsequently.

4.3. Effect of the spring coefficient for the horizontal constraint

In the panel installation, the stiffness of the horizontal constraint can be controlled by the tightness and thickness of the rubber cushion. The spring coefficient of a clamp with a rubber cushion can be characterized by a tension test. When $\mu \to 0$, no horizontal constraint can be provided by the support, and the present model is reduced to the classic beam model due to no axial force exists. When $\mu > 0$, the horizontal force will increase with the curvature of the beam, and thus produce a nonlinear effect on the deflection. This subsection studies the effect of μ on the deflection of SSFF and CCFF panels.

Figure 5 shows the deflection of the SSFF panel for varying spring stiffness (μ) values at $0, 10^6, 10^7, 10^8, 10^9$N/m and infinity, respectively. The deflection is linear for the case of zero spring coefficient (no horizontal constraint) and is nonlinear for a spring stiffness greater than zero. In addition, the deflection decreases significantly as the spring stiffness increases. For example, the deflection, for a load of 20KPa, decreases from 112.4 to 10.13mm for $\mu = 0$ to ∞, respectively. The effectiveness of the horizontal constraint is superior in a certain range of the spring coefficient, such as $10^6 - 10^8$N/m. Beyond this range, the bending behavior of the panel is convergent to the case of either zero or infinity of the spring coefficient. For a frameless BIPV panel attached to a

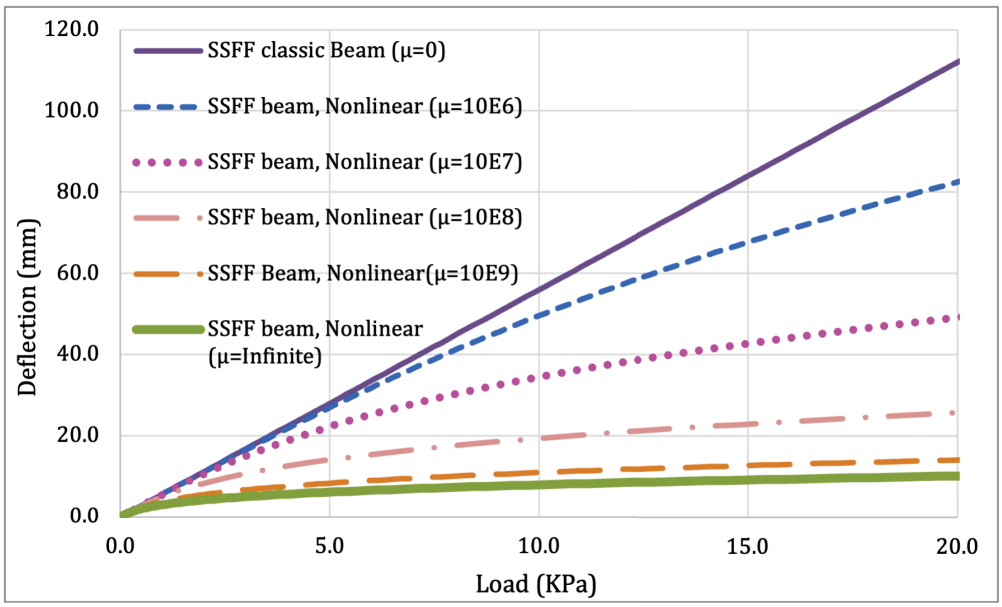

Figure 5: The deflection of the center of an SSFF panel ($\overline{EI} = 2060\text{N.m}^2$) for varying μ values

supporting structure, SSFF can be a good approximation because the panel's rotation at the end cannot be well constrained. From a framed panel, the clamps of the frame can be fixed onto the supporting structure, so that the rotational angle will be fixed, which is demonstrated in the CCFF configuration. The rubber cushion can still provide horizontal constraints similar to the case of SSFF.

Figure 6 shows the deflection of the CCFF panel with a much larger loading range in comparison with Figure 5. Because of the stronger constraint of the clamped support, the nonlinear behavior starts at a higher load. For the spring coefficient changing from $\mu = 0$ to ∞, the clamped support changes from a roller clamp to a perfectly rigid connection. The deflection of the CCFF beam decreased from 101.3mm to 15.65mm, for $\mu = 0$ to ∞, respectively, for a load of 90KPa. Hence the deflection of the CCFF beam decreased by 84.5% from zero horizontal constraints to infinitely rigid constraints. The sensitivity of the deflection to the spring coefficient of the horizontal constraint changes in comparison with the SSFF counterpart. For the spring coefficient beyond the region $10^7 - 10^9$ N/m, the bending behavior of the panel is convergent to the case of either zero or infinity of the spring coefficient. Therefore, BIPV panels can be significantly stiffened by introducing horizontal constraints and restricting the rotational angle.

In both CCFF and SSFF beams, the deflection is linear for the case of zero spring coefficient (no horizontal constraint) and is nonlinear for a spring stiffness greater than zero. The present model converges to the classic beam theory for both boundary conditions at $\mu = 0$, but provides a

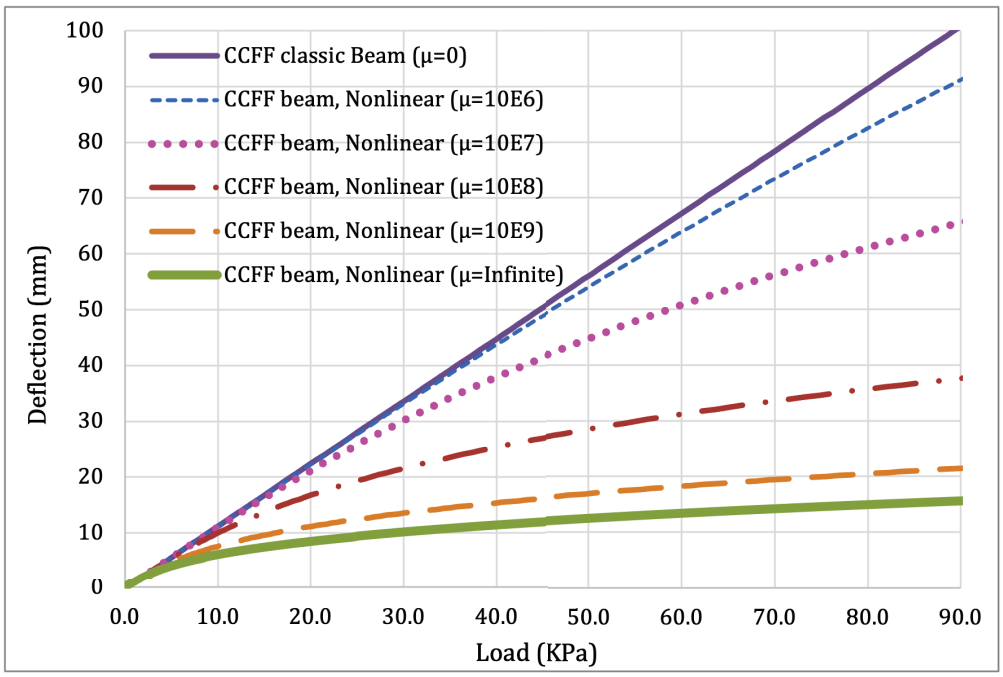

Figure 6: The deflection of the center of a CCFF panel ($\overline{EI} = 2060\text{N.m}^2$) for varying μ values

new solution for $\mu > 0$ taking into account the nonlinear behavior.

5. Application of the present theory to the BIPV panel design

5.1. Design procedure of BIPV panels under surface load

As the solar energy industry has been booming in the past decade in the United States and around the world, BIPV is a major part of the solar energy industry. Because the BIPV panels become a part of the structure, the design and analysis of the material and structural aspects of BIPV panels are critical for the safety and performance of the BIPV system. Particularly, large solar panels with the solar cells encapsulated in the EVA or other encapsulants have become a standard in the solar energy building industry. Indeed, the compliant encapsulant layer provides protection to solar cells, which release the in-plane stress. However, the bending of solar panels will create stress variation along the thickness, which leads to microcracks, efficiency reduction, and an immature lifetime of solar cells. Therefore, the analysis of the deflection of large BIPV panels is not only of significance to structural design for architectural and safety requirements, but also critical for energy efficiency and lifetime assurance of the BIPV systems.

Particularly, for some specially designed BIPV systems, customized BIPV panels are required with certain specifications. Because no specific building code exists for PV module design [8, 11],

large safety factors have been used with conservative design methods, which leads to very heavy solar modules. However, thicker glass sheets may not lead to higher safety but they increase the panel's life cycle cost. The present theory creates a quantitative method to stiffen BIPV panels by providing horizontal constraints on the supports along the opposite edges, and thus enables the use of lightweight dual-glass solar panels through the following procedure:

1. Given the load conditions and building architectural features, the supporting structure of the BIPV system can be designed to pass the roof load through the building frame to the foundation;
2. Given the span of solar panels in accordance with the supporting structure, the mounting system of the BIPV panel can be selected and spring coefficients of the clamps can be determined by the cushion types and the tightness;
3. Given the soft core material configuration, the flexural rigidity of solar modules changing with the glass thickness can be characterized;
4. The glass thickness can be determined by extreme loading conditions with the classic beam theory by the maximum deflection and material strength;
5. The present nonlinear beam theory can be used to optimize the design with an appropriate spring coefficient of the clamp with rubber cushion for SSFF and CCFF;
6. A mock test of the optimized design of the BIPV panel can be performed for the validation and verification of the design.

The present model can predict both the deflection and stress distribution by Eqs. (6) and (22) with parameters in Eqs. (9) and (19) for SSFF and CCFF respectively. The formulation provides a large variation range of the design parameter μ for both SSFF and CCFF and enables accurate prediction of the deflection of the solar panel supported by two opposite edges.

5.2. Case study: the design of a BIPV panel

This section demonstrates the structural design of a BIPV canopy to be built in Worcester, Massachusetts, USA, where we have collaborated with the BIPV panel manufacturer. The classic beam and the present nonlinear theory are used for the panel design, which is a part of the roof structure.

Following the steps illustrated in Section 5.1, the design procedure is as follows:

1. Material property, loading and support condition:

   Material property: Two types of 1.524m (60in) × 2.032m (80in) tempered laminated glasses with EVA interlayer are analyzed in this study; Module A and Module B. Module A has a total thickness of 14.3mm (9/16″) including 6.35mm (1/4″) for both top and bottom glass layers, and 1.6mm (1/16″) thick EVA interlayer; while Module B has a total thickness of 17.5mm(11/16″) including 6.35mm (1/4″) thick top glass, 9.53mm (3/8″) bottom glass layers and 1.62mm (1/16″) thick EVA interlayer. The material properties of Module A and Module B are shown in Tables 2 and 3, respectively.

Material	thickness (mm)	Young's Modulus (MPa)	Poisson Ratio
Glass	6.35	7.17×10^4	0.22
EVA	1.6	15.17	0.4
Glass	6.35	7.17×10^4	0.22

Table 2: Material properties of Module A

Material	thickness (mm)	Young's Modulus (MPa)	Poisson Ratio
Glass	6.35	7.17×10^6	0.22
EVA	1.6	15.17	0.4
Glass	9.53	7.17×10^6	0.22

Table 3: Material properties of Module B

   Loading condition: The glass panels are designed using the allowable stress design by considering different load cases. For this study, we focus on a load case that combines dead, live and snow loads which are uniformly distributed on the glass panel. The glass panels are subjected to roof snow load of 2250Pa (0.326Psi) in addition to their own weight and live loads. In total, the panel is designed for a combined loading of 3482Pa (0.505Psi).

   Support condition: The laminated glass is supported by structural frames that do not interfere with maximum expansion and contraction . The modules are roller supported on two opposite edges and free on the other two sides.

2. Determination of the spring coefficients of the clamps:

   The spring coefficient of the clamps will be assumed to be fully rigid, thereby $\mu = \infty$, which can be achieved by the smart mounting system elaborated subsequently.

3. Determining the flexural rigidity of the laminated glass:

   The flexural rigidity of the modules is calibrated by using the design deflection calculated

using the classic beam theory. As discussed in the previous sections, the effective flexural rigidity of laminated glasses with a soft core is much less than the values calculated using the classic composite beam theory. Accordingly, the calibrated $\overline{EI}$ for module A is 31.8 KN.m^2, and for module B, the $\overline{EI}$ is 54.5 KN.m^2.

4. Glass thickness determination

   The design requirement for the deflection is that the allowable deflection is less than $19.05mm$ ($0.75''$). The design used the classic beam theory to determine the deflection of these laminated glasses and the maximum deflection for the design load of 3482Pa (0.505Psi) for Module A and B is 17.145mm ($0.675''$) and 13.13mm ($0.399''$), respectively. The deflections of both modules are below the allowable deflection of 19.05mm ($0.75''$), thereby satisfying the design requirement.

5. Optimizing the design using the new nonlinear formulation

   The design of the laminated glass can be optimized by considering the effect of the rubber cushions on the opposite edges of the support. The effect of the horizontal constraints will be considered for these simply supported laminated glasses (SSFF) and the spring coefficient of the clamp will be assumed to be fully rigid.

   Using the formulation in section 3.2, Eq.(15) the deflection of Module A is 8.35mm ($0.329''$), which is approximately 51% less that the deflection calculated for the design using the classic beam theory. For Module B the deflection reduces to 6.68mm ($0.263''$) using the nonlinear analysis, which is a 34% decrease from the design deflection. It is very clear that the laminated glass thickness used for the analysis and design of these laminated glasses is much larger than needed and can be further reduced considering the type and tightness of the cushion.

   The glass thickness can be optimized by using the formulation and making sure that the allowable deflection limit of 19.05mm ($0.75''$) isn't exceeded; For Module A, by decreasing the glass thickness from 6.35mm ($0.25''$) to 3.81mm ($0.15''$), a 40% material decrease, we achieve a deflection of 11.4mm ($0.45''$) which is well below the limiting deflection of 19.05mm $0.75''$. For Module B, by decreasing the thickness of the top glass from 6.35mm ($0.25''$) to 3.81mm ($0.15''$) and the lower glass from 9.525mm ($0.375''$) to 3.81mm ($0.15''$), a 52% decrease in glass material, the deflection reduces to 9.9mm ($0.39''$), which too is well below the allowable deflection. Hence we can conclude that laminated glass can be stiffened by accounting for the effect of the glass support that is determined by cushion type and tightness, thereby decreasing the glass thickness that is needed to sustain the loads that the laminated glass will

be subjected to in it's lifetime.

6. The optimized design can be validated by performing a mock test of the laminated BIPV module.

5.3. A smart mounting system of solar panels for BIPV systems

The discovery of the stiffening BIPV module by the horizontal constraint motivates an invention of a smart mounting system for solar panel installation and construction [32]. This invention is to design a stiff support fixture of large BIPV panels, which is integrated with a smart sensor-controlled motor. By adjusting the tension applied by the motor, the fixture first keeps the dimension of solar modules unchanged under temperature and mechanical loading, and thus minimizes the stress concentration due to the material difference in the layered structure. The lifetime of the brittle solar cells will be significantly extended with less micro-cracks and deformation. The spacing between the modules remains constant in the service life so that the silicone connection between modules will lasts longer without thermal fatigue or water leakage from the roof. In addition, the fixture increases the stiffness of the solar module by adding tension to the solar module via mountings on the two sides. As a result, the deflection of the module can be reduced, so thinner, lighter modules are allowed for architectural and economic benefits.

The mounting fixture can be installed in the construction field as a part of the construction procedure or in the manufacturing plant for modular manufacture and construction. Compared with the simply supported BIPV panels without horizontal constraint or forces, this smart mounting fixture can significantly reduce the deflection of the panel under external loading.

As shown in Figure 7, once a module is laminated in Fig. 7(a), two end clamps are installed at the opposite ends. A frictional pressure clamp with strong glue or rubber contact cushion can be used in Fig. 7(b).

For stiffer connections, prefabricated holes in glass with bolts can be used as well. The number and size of the holes shall be carefully designed and verified to avoid damage when a load is applied to the hole. A central column is installed underneath the module, connecting with the mid-points of the two clamps. One side of the column is a rigid connection, and the other is connected with a smart cushion. The column does not have to fully contact with the module, but can provide vertical support when the module exhibits large deflection, particularly in the mid-range for redundant protection. The smart cushion can push the two end clamps so as to apply tension to the panel and keep a constant spacing distance between the end clamps to avoid any leakage problems.

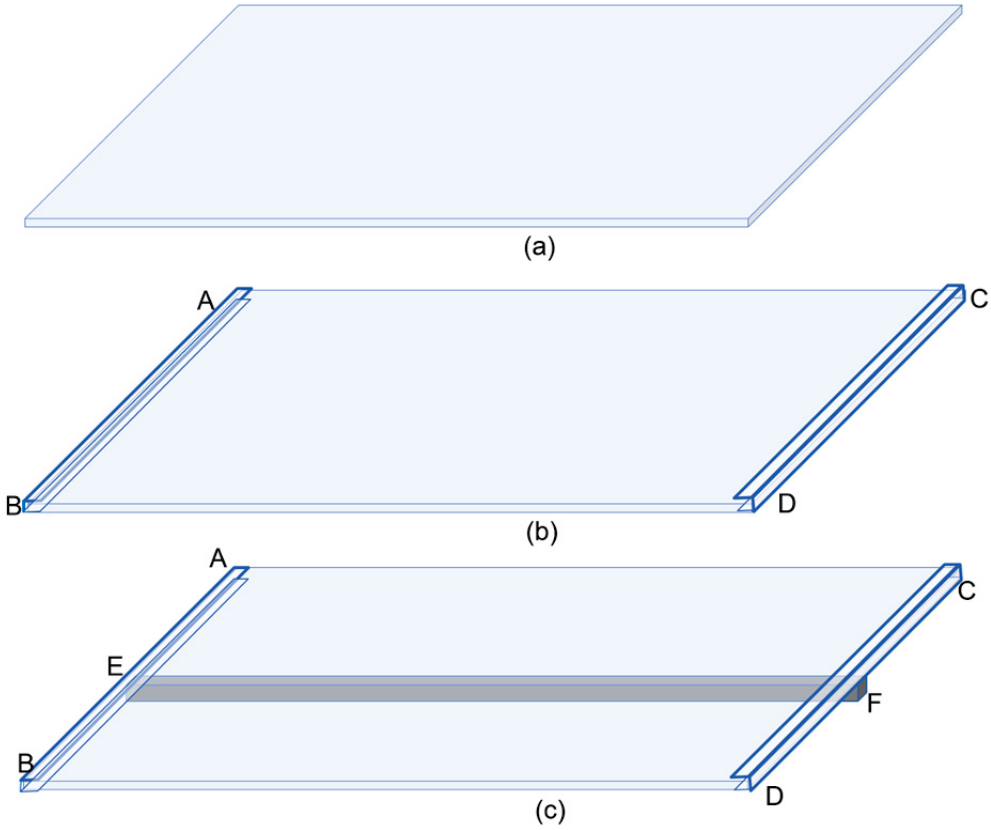

Figure 7: The layout of the mounting fixture for a BIPV module. (a) a laminated BIPV module; (b) install two end clamps AB and CD with pressure-glue connection or bolted connection, and; (c) install a mid-column EF for support and pretension of the module.

Given a climate zone, we can estimate the highest temperature (T_{max}) in the area, so that we can calculate the natural length (L_0) of the module at the temperature. Although the design method is general for any size of modules, for the clarity of description, we use a module with a size of 1m (width)×2m (length)= 2m^2 (area) as an example, or $L_0 = 2$m at T_{max}.

The module size will be adjusted to $L_0 = 2$m by a smart motor-driven cushion, and panels will be installed on the roof structure with a fixed gap g_0 (in the range of $3 - 6$mm), which is generally filled with transparent silicone such as polydimethylsiloxane(PDMS). For panels mounted by conventional fixtures, the gap will change with the weather and mechanical load. When PDMS is aged with degradation, the gap may become a crack during the thermal cycling load, which will lead to roof leakage. The mechanical and electrical design of the smart cushion is elaborated as follows:

To strengthen the solar panel and keep the panel length as well as the gap distance constant, a self-sensing and control device is invented in Figure 8. At the interface of the connection line, A and B are two hinge points fixed on the clamps with a distance a_0 in a range of $20 to 40$mm, which include a buffer gap between the clamps at 2 mm. Note that in general the buffer gap is 10 to 20mm filled with solar panel sealant, which is subjected to thermal cycle loading with a lifetime of 10 to 15 years; while the smart mounting system enables a very small gap change so that 1mm thick of silicone coating on the clamp surface can maintain the seamless roof without sealant. Four links with rigid bars are installed with an equal angle of 90 degrees, although other angles can also be selected such as 60 or 120 degrees. Therefore the distance of CD is also a_0. C and D are two electrodes that connect a motor in the smart cushion with a screw block. When the current is in the direction of the green arrow from left to right, the motor drives the cushion to push the two clamps connected with A and B away from each other and increase the force on the central column that pushes the two clamps mounted on each side of the panel; whereas when the current is in the direction of the red arrow, the motor drives the cushion in the opposite direction to move the two clamps connected with A and B closer to each other and reduce the force on the central column. Four electrodes are installed on the line connecting points C and D: Two green electrodes are installed on the outside distance between C and D and two red electrodes within the distance between C and D. A battery is connected with the green and red electrodes as Figure 8. The four electrodes are in the same line of CD and exhibit a distance $\Delta = 0.2$mm to the electrode C or D.

The working mechanism of this smart mounting fixture is achieved as below:

1. At the initial condition, we set up the highest working temperature T_{max} for the region. For

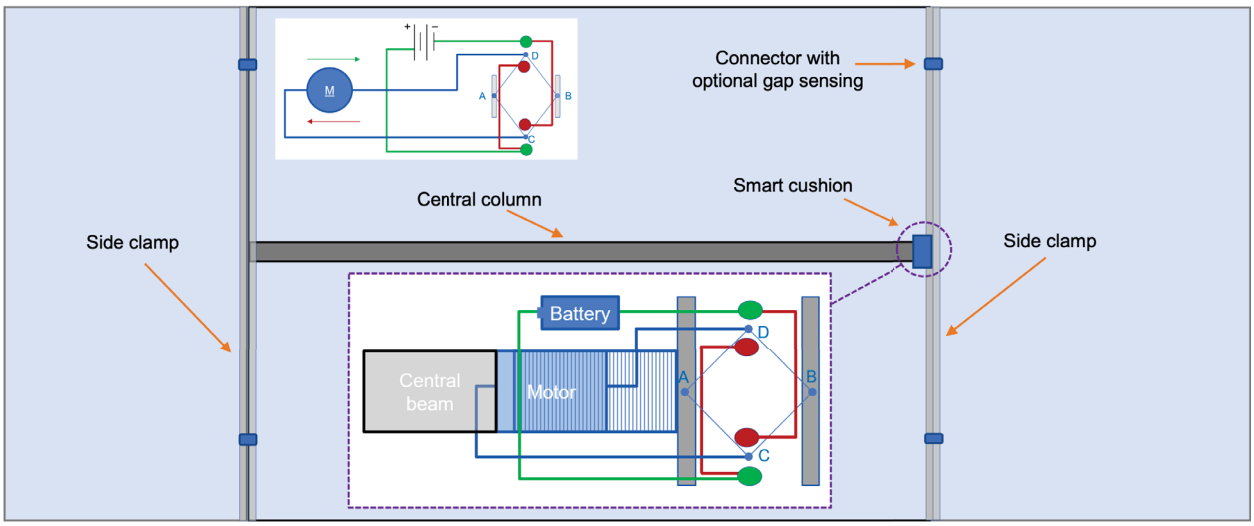

Figure 8: The connection of the smart mounting fixture with self-sensing and control of the dimension of the module

example, $T_{max} = 90°C$ for New York state on the roof. We can calculate the length of the module at $T_{max} = 90°C$ as L_0. Even if the temperature is different on the installation day, we can still use the smart cushion to adjust the width to L_0, which means when the temperature reaches T_{max}, the smart cushion exhibits zero force and the central column perfectly is in contact with the right clamp.

2. During the installation, modular construction is used. The module with the fixture at the width L_0 will be installed onto the roof with enough horizontal support to stabilize the fixture, use the connectors to link the sections together. A gap sensing and control unit is installed with the connectors for monitoring and controlling the gap.
3. The self sensing and control unit is installed along with the interface next to the smart cushion with the circuit shown in Figure 8, in which the lower inset shows the geometry and the upper inset provides the circuit connection.
4. When the module experiences contraction by a temperature decrease, the distance between the two clamps mounted on two sides of the panel decreases. As a result, AB decreases, and electrodes C and D move away from each other and touch the green electrodes, which triggers the motor to increase the force on the central column to push the two side clamps away from each other, so that AB can recover the initial distance and the electrodes become disconnected.
5. When the module experiences expansion by a temperature increase, the distance between the two side clamps increases, and AB increases, electrodes C and D move toward each other and

touch the red electrodes, which triggers the motor to reduce the forces on the central column, so that AB can recover the initial distance and the electrodes become disconnected.

6. Because the initial distance of AB is set up at the highest working temperature, the smart cushion will not experience any force at the highest temperature. At lower temperatures, there is pre-tension in the panel module and compression in the central column to main the initial distance, the gap between the modules will stay constant.

Note that because the loading cycle on the roof is slow, the smart cushion system is triggered at a very low frequency. The lifetime of the battery is expected to be 5 to 10 years. Therefore the battery recharge or replacement of this smart mounting system every 5 years can be scheduled. To save the number of motors, one row of BIPV modules can be rigidly connected into one piece sharing one motor. This smart mounting system makes the modules into a seamless roof. It not only reduces the material manufacture and construction costs, but creates the feasibility of a permanent roof with a lifetime of over 40 years by reducing the thermal fatigue of solar cells and preventing water leakage problems. Long-term performance tests and life-cycle cost analysis will be underway.

6. Conclusions

The present model considers the horizontal constraint and predicts the nonlinear mechanical behavior of large BIPV panels supported along two opposite edges. Due to the membrane force, the deflection of a panel can be much smaller than the prediction of the classic beam or plate theories, which enables new panel design with thinner glass layers. The theoretical model presented in this study can serve as a fundamental basis to understand the nonlinear behavior of BIPV panels, providing design guides for the structural design and analysis of these laminated panels. The present model predicts the previous experimental results very well, which shows a difference of over 20% from the classic beam theory under a load of at 4KPa. When the load is higher, the difference can reach about 90%. Given the panel configuration in the experiments, the sensitive range of the spring coefficient is different for varying boundary conditions of SSFF and CCFF at $10^6 - 10^8$ N/m and $10^7 - 10^9$ N/m, respectively. The case study shows over 40% savings of glass can be achieved by using the horizontal constraint, which leads to the invention of a smart mounting system for BIPV roof installation and construction. By self-sensing the gap change between modules, the smart cushion drives the module with horizontal force to merge the gap, so as to maintain a seamless

roof adapting to the environmental and mechanical loading. The present formulation can be used in future BIPV roof design and analysis for the nonlinear elastic deflection of the solar panels by the horizontal constraint.

Declaration of competing interest

The authors declare that they have no known competing financial interests or personal relationships that could have appeared to influence the work reported in this paper.

Funding

This work is sponsored by the National Science Foundation IIP # 1738802, IIP # 1941244, CMMI# 1762891, and U.S. Department of Agriculture NIFA # 2021-67021-34201 whose support is gratefully acknowledged.

Acknowledgment

The authors thank Mr. Yanchu Zhang and Dr. Chunlin Wu for the fruitful discussion and preliminary work on this study. In addition, we are grateful to Mr. Frank Pao and Mr. Joe Morrissey for sharing the industry applications with the team.

Data Available Statement

All data that support the findings of this study are available from the corresponding author upon reasonable request.

References

[1] H. Yin, M. Zadshir, F. Pao, Building Integrated Photovoltaic Thermal Systems: Fundamentals, Designs and Applications, Academic Press, 2021.

[2] A. Ghosh, Potential of building integrated and attached/applied photovoltaic (bipv/bapv) for adaptive less energy-hungry building's skin: A comprehensive review, Journal of Cleaner Production 276 (2020) 123343.

[3] D. Yang, H. Yin, Energy conversion efficiency of a novel hybrid solar system for photovoltaic,

thermoelectric, and heat utilization, IEEE Transactions on Energy Conversion 26 (2) (2011) 662–670.

[4] Q. Lin, F. Chen, H. Yin, Experimental and theoretical investigation of the thermo-mechanical deformation of a functionally graded panel, Engineering Structures 138 (2017) 17–26.

[5] K. Naumenko, V. A. Eremeyev, A layer-wise theory of shallow shells with thin soft core for laminated glass and photovoltaic applications, Composite Structures 178 (2017) 434–446.

[6] S. Ravyts, M. Dalla Vecchia, G. Van den Broeck, J. Driesen, Review on building-integrated photovoltaics electrical system requirements and module-integrated converter recommendations, Energies 12 (8) (2019) 1532.

[7] T. Zhang, L. Xie, Y. Li, T. K. Mallick, Q. Wei, X. Hao, B. He, Experimental and theoretical research on bending behavior of photovoltaic panels with a special boundary condition, Energies 11 (12) (2018) 3435.

[8] Y. Li, L. Xie, T. Zhang, Y. Wu, Y. Sun, Z. Ni, J. Zhang, B. He, P. Zhao, Mechanical analysis of photovoltaic panels with various boundary condition, Renewable Energy 145 (2020) 242–260.

[9] M. Z. Aşık, S. Tezcan, A mathematical model for the behavior of laminated glass beams, Computers & Structures 83 (21-22) (2005) 1742–1753.

[10] S. Misara, A. Pornnimit, Mechanical characteristics of bipv modules under different load scenarios and encaplsuations, in: International Solar Energy Society-ISES-30th ISES Biennial Solar World Congress 2011, 2011, pp. 2193–2203.

[11] X. Menga, D. Zhangb, P. Fengb, N. Huc, Review on mechanical behavior of solar cells for building integrated photovoltaics, renewable energy 15 (2021) 16.

[12] IEC61215-2005, Crystalline silicon terrestrialw photovoltaic (pv) modules [s], International Electrotechnical Commission (2005).

[13] IEC63092-1-2020, Photovoltaics in buildings - part 1: Requirements for building-integrated photovoltaic modules, International Electrotechnical Commission (2020).

[14] IEC63092-2-2020, Photovoltaics in buildings - part 2: Requirements for building-integrated photovoltaic systems, International Electrotechnical Commission (2020).

[15] C. Peng, Y. Huang, Z. Wu, Building-integrated photovoltaics (bipv) in architectural design in china, Energy and buildings 43 (12) (2011) 3592–3598.

[16] S. Dietrich, M. Pander, M. Ebert, J. Bagdahn, Mechanical assessment of large photovoltaic modules by test and finite element analysis, in: 23rd European Photovoltaic Solar Energy Conference. Valencia, Spain, 2008.

[17] L. Sable, D. Kinsella, M. Kozlowski, Influence of eva, pvb and ionoplast interlayers on the structural behaviour and fracture pattern of laminated glass, International journal of structural glass and advanced materials research 3 (2019) 62–78.

[18] K. Naumenko, V. A. Eremeyev, A layer-wise theory for laminated glass and photovoltaic panels, Composite Structures 112 (2014) 283–291.

[19] J. Eisenträger, K. Naumenko, H. Altenbach, H. Köppe, Application of the first-order shear deformation theory to the analysis of laminated glasses and photovoltaic panels, International Journal of Mechanical Sciences 96 (2015) 163–171.

[20] S.-H. Schulze, M. Pander, K. Naumenko, H. Altenbach, Analysis of laminated glass beams for photovoltaic applications, International Journal of Solids and Structures 49 (15-16) (2012) 2027–2036.

[21] P. Foraboschi, Analytical model for laminated-glass plate, Composites Part B: Engineering 43 (5) (2012) 2094–2106.

[22] M. Weps, K. Naumenko, H. Altenbach, Unsymmetric three-layer laminate with soft core for photovoltaic modules, Composite Structures 105 (2013) 332–339.

[23] S. Timoshenko, S. Woinowsky-Krieger, et al., Theory of plates and shells, Vol. 2, McGraw-hill New York, 1959.

[24] D. N. Arnold, A. L. Madureira, S. Zhang, On the range of applicability of the reissner–mindlin and kirchhoff–love plate bending models, Journal of elasticity and the physical science of solids 67 (3) (2002) 171–185.

[25] I. Elishakoff, Handbook on Timoshenko-Ehrenfest beam and Uflyand-Mindlin plate theories, World Scientific, 2020.

[26] J. Hu, W. Chen, B. Zhao, H. Song, Experimental studies on summer performance and feasibility of a bipv/t ethylene tetrafluoroethylene (etfe) cushion structure system, Energy and Buildings 69 (2014) 394–406.

[27] J. Kurnik, M. Jankovec, K. Brecl, M. Topic, Outdoor testing of pv module temperature and performance under different mounting and operational conditions, Solar Energy Materials and Solar Cells 95 (1) (2011) 373–376.

[28] A. J. Beinert, M. Ebert, U. Eitner, J. Aktaa, Influence of photovoltaic module mounting systems on the thermo-mechanical stresses in solar cells by fem modelling, in: Proceedings of the 32nd European Photovoltaic Solar Energy Conference and Exhibition, Munich, Germany, 2016, pp. 1833–1836.

[29] W. Chen, L. Luo, Z. Guo, P. Yuan, Experimental studies on load-carrying capacity of hfr-lwc beams accompanying membrane action, Engineering Structures 228 (2021) 111497.

[30] L. Chen, Q. Fang, Z. Guo, J. Liu, An improved analytical method for restrained rc structures subjected to static and dynamic loads, International Journal of Structural Stability and Dynamics 14 (01) (2014) 1350052.

[31] W. Chen, L. Luo, Z. Guo, Y. Wang, Load-carrying capacities of fully clamped rc slab accompanying compressive-tensile membrane actions: A theoretical approach, International Journal of Structural Stability and Dynamics 20 (08) (2020) 2050094.

[32] H. Yin, F. Pao, J. Lou, M. Zadshir, Solar personal rapid transit system with autonomous pods - building integrated photovoltaic thermal systems, u.S. Patent App. 63248502 (September 2022).